Effective transmission conditions across a resonant bubbly metascreen

Kim Pham[1]† , Jean-Francois Mercier[2], Daniel Fuster[3], Agnès Maurel[4], Jean-Jacques Marigo[5],

[1]IMSIA, CNRS, ENSTA ParisTech, 828 Bd des Maréchaux, 91732 Palaiseau, France,
[2]Poems, CNRS, ENSTA ParisTech, INRIA, 828 Bd des Maréchaux, 91762 Palaiseau, France,
[3]Institut d'Alembert, CNRS, Univ. Paris 6, 4 place Jussieu, 75005 Paris, France,
[4]Laboratoire de Mécanique des Solides, CNRS, Ecole Polytechnique, 91120 Palaiseau, France,
[5]Institut Langevin, CNRS, ESPCI ParisTech, 1 rue Jussieu, 75005 Paris, France,

(Received xx; revised xx; accepted xx)

Our study concerns the propagation of acoustic waves through a thin screen made of a periodic arrangement of air bubbles in water. The analysis is performed in the time-domain using matched asymptotic expansion technique similar to that presented in Miksis & Ting (1989). The resulting model involves effective transmission conditions, which encapsulate the effect of the bubbly screen in a non intuitive jump of the normal velocity. This velocity jump is linked to a continuous version of the bubble radius satisfying an equation of the Rayleigh-Plesset's type. Numerical implementation of the effective model allows us to discuss the influence of the distance inter bubbles within the screen and that of the non linearities on the propagation of an acoustic pulse.

Key words: Air bubbles in water, Rayleigh-Plesset equation, locally resonant metascreen, Minnaert resonances, Homogenization, Matched Asymptotic Expansion.

1. Introduction

In 1985, Caflisch and co-workers analyzed the wave propagation in bubbly liquids (Caflisch *et al.* 1985*a*,*b*) offering a rigorous mathematical framework to the former analysis developed by Van Wijngaarden (1968). Using asymptotic analysis, they derived an effective wave equation involving a continuous version of the bubble radius satisfying an equation of the Rayleigh-Plesset's type. Once linearized in the harmonic regime, they exhibited an effective sound speed being frequency dependent with strong variations in the vicinity of the Minnaert frequency.

In some practical situations, the region of bubbles is reduced to one or a few layers. The most famous example are the anechoic tiles, codenamed Alberich, developed during the Second World War by the german marine; these tiles are the building blocks of a rubber net containing bubbles used to block the signals of sonars (Gaunaurd 1977). It is also the case of bubble nets used to protect underwater structures from damage by underwater explosions (Domenico 1982) or those created by some of the marine mammals to catch fish (Leighton 2004). Recently, these metascreens with subwavelength thickness have been revisited in the context of metamaterials. Resonant bubbles are

† Email address for correspondence: kim.pham@ensta-paristech.fr

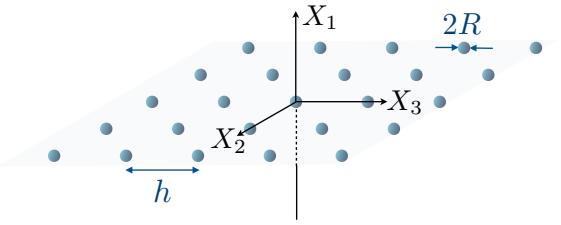

FIGURE 1. The actual problem: a bubbly screen in the $X_1 = 0$-plane with spacing h.

the equivalent of split rings in electromagnetism and by designing judiciously their structuration, it should be possible to obtain exotic properties as those obtained for their electromagnetic counterparts. Leroy *et al.* (2009) realized controlled experiments to study the transmission of ultrasounds through a single layer of bubbles in water; Bretagne *et al.* (2011) realized a bubble raft close to an interface with air or sandwiched in air and analyzed the effects of such interfaces; in Leroy *et al.* (2015), the ability of the metascreens to produce superabsorption has been demonstrated. These experimental findings are supported by a model based on physical arguments, see also Sharma *et al.* (2017). Ng & Ting (1986) and Miksis & Ting (1989) used the effective wave equation derived in Caflisch *et al.* (1985*a*,*b*) in the limiting case of thin layers. We also mention the work of Ammari *et al.* (2017) which provides almost exact expressions of the scattering coefficients in the harmonic regime within a rigorous mathematical framework.

In this study, we present an asymptotic analysis similar to that of Miksis & Ting (1989) for a bubbly metascreen. The calculations are performed in the time domain and preserving the non linear behavior of the bubble oscillations, see §2 where the actual problem is presented and §3 where the scaling is set. The derivation of the effective transmission conditions is detailed in §4. It relies on multiple scale homogenization combined with matched asymptotic analysis. Because of the small thickness of the screen, the analysis leaves us with effective transmission conditions (instead of an effective wave equation); while the pressure is continuous across the screen, the normal velocity satisfies a non intuitive transmission condition involving a continuous version of the bubble radius satisfying an equation of the Rayleigh-Plesset's type. Such transmission conditions have been obtained in Ng & Ting (1986) in the linear regime and in Miksis & Ting (1989) in the non-linear regime and this is discussed in §5, along with the analysis of the equation of energy conservation in the effective problem and the analysis of the radiative damping of the bubbles in terms of an effective viscosity. Eventually, we present in §6 numerical results which exemplify the interaction of an acoustic wave train with bubbly screens; in particular, the influence of the spacing between bubbles and of the non-linearities are discussed.

2. The actual problem

We consider wave propagation in a liquid containing an array of gas bubbles, typically air bubbles in water (figure 1). Let ρ, $P_{\rm tot}$ and $\mathbf{U}$ be the density, the total pressure and the velocity, functions of the space $\mathbf{X}$ and of the time t. At $t = 0$, the system is at equilibrium with

$$P_{\rm tot}(\mathbf{X}, 0) = P_{\rm eq}, \quad \rho(\mathbf{X} \in \text{liquid}, 0) = \rho_\ell \quad \rho(\mathbf{X} \in \text{gas}, 0) = \rho_{\rm g}, \quad \mathbf{U}(\mathbf{X}, 0) = \mathbf{0}, \qquad (2.1)$$

and we denote $P = (P_{\rm tot} - P_{\rm eq})$ the acoustic pressure. The acoustic source is switched on afterwards, for $t > 0$, waves propagate in the liquid and through the bubble screen.

Assuming that the viscosity and the surface tension can be neglected and that the flow remains irrotational, $(\rho, P, \mathbf{U})$ satisfy the Euler equations

$$\begin{cases} \dfrac{\partial \rho}{\partial t} + \operatorname{div}(\rho \mathbf{U}) = 0, \quad \rho\left(\dfrac{\partial \mathbf{U}}{\partial t} + (\mathbf{U}\cdot\nabla)\mathbf{U}\right) = -\boldsymbol{\nabla} P, \\ \quad \nabla \wedge \mathbf{U} = 0. \end{cases} \tag{2.2}$$

For a nearly incompressible liquid and a perfect gas under adiabatic transformations (see *e.g.* Bergamasco & Fuster (2017) for a discussion on the validity of the adiabatic regime), the equations of state are written in the form

$$\begin{cases} P_{\text{tot}} = P_{\text{eq}} + c_\ell^2(\rho - \rho_\ell), & \text{in the liquid,} \\ \dfrac{P_{\text{tot}}}{P_{\text{eq}}} = \left(\dfrac{\rho}{\rho_{\text{g}}}\right)^\gamma, & \text{in the gas, with } c_{\text{g}}^2 = \dfrac{\gamma P_{\text{eq}}}{\rho_{\text{g}}}, \end{cases} \tag{2.3}$$

where $\rho_{\ell,\text{g}}$ and $c_{\ell,\text{g}}$ are the mass density and the sound speed in the fluid and in the gas at the equilibrium with pressure P_{eq}, and with γ the adiabatic index. Finally, we assume that the bubbles remain spherical, an assumption motivated by the fact that wavelengths are much larger than the bubbles and thus, they impose an almost uniform pressure at the scale of a single bubble. The waves hitting the bubble i produce its oscillation, hence a time variation of its radius $R_i(t)$ around R_{eq}, its value at equilibrium. At the interface with the liquid, the radius of the bubble i is dictated by the condition

$$\mathbf{U}(\mathbf{X}, t)\cdot\mathbf{n} = \dot{R}_i(t), \tag{2.4}$$

where the dot denotes the time derivative.

3. Scalings and non dimensional form of the problem

Let U_0 be the amplitude of the acoustic velocity. If we denote U_0 the typical amplitude of the acoustic velocity, we have, from (2.2),

$$U \sim U_0, \quad (\rho - \rho_\ell) \sim \rho_\ell\, Ma, \quad P \sim \rho_\ell c_\ell^2\, Ma, \quad \text{with } Ma = \frac{U_0}{c_\ell}, \tag{3.1}$$

the Mach number measuring the amplitude of the acoustic velocity with respect to the speed of sound. In the following, we shall use a non dimensional form of (2.2). We define the non dimensional time τ and space variable $\mathbf{x}$ as

$$\tau = \omega t, \quad \mathbf{x} = \frac{\omega}{c_\ell}\mathbf{X}, \tag{3.2}$$

where ω is the typical frequency imposed by the source. Motivated by (3.1), the non dimensional acoustic fluctuations in pressure p, mass density ϱ and velocity $\mathbf{u}$, and the bubble radius R, are defined by

$$p = \frac{1}{\rho_\ell c_\ell^2\, Ma}\, P, \quad \varrho = \frac{1}{\rho_\ell Ma}\left(\rho - \rho_{\ell,\text{g}}\right), \quad \mathbf{u} = \frac{1}{c_\ell Ma}\,\mathbf{U}, \quad \mathsf{R} = \frac{R}{R_{\text{eq}}}. \tag{3.3}$$

In the low frequency regime, the maximum wavelength c_ℓ/ω imposed by the source is much larger than h and R_{eq}. This is measured by the small parameter ε

$$\varepsilon = \frac{\omega}{c_\ell} h \ll 1. \tag{3.4}$$

Next we impose the following scalings for the bubble radius, contrasts in the mass densities and bulk moduli (gas and liquid), and for the Mach number

$$\frac{\omega}{c_\ell} R_{\rm eq} = \mathsf{r}_{\rm eq}\varepsilon^2, \quad \frac{\rho_{\rm g}}{\rho_\ell} = \alpha\varepsilon^4, \quad \frac{\rho_{\rm g} c_{\rm g}^2}{\rho_\ell c_\ell^2} = \beta\varepsilon^4, \quad Ma = m\varepsilon^4. \tag{3.5}$$

Doing so, we assume that the bubble radius is much smaller than the array spacing with $R_{\rm eq}/h = O(\varepsilon)$. Such separation of scales was already used in Caflisch *et al.* (1985*b*) for bubbly liquid, and in this case, the separation was even more demanding with $R_{\rm eq}/h = O(\varepsilon^2)$. The scaling for the contrast in the mass densities guaranties that resonances can take place; the scaling on the contrast in the bulk moduli simply follows since the sound speeds in liquids and gases do not differ significantly. Finally, the scaling for the Mach number is dictated by the scaling for the contrast in mass density, as in Caflisch *et al.* (1985*b*). The problem now reads as

$$\text{in the gaz:} \quad \begin{cases} \dfrac{\partial \varrho}{\partial \tau} + \varepsilon^4 \Big(\alpha \mathrm{div}\mathbf{u} + m \mathrm{div}(\varrho \mathbf{u}) \Big) = 0, \\ \varepsilon^4 (\alpha + m\varrho) \left(\dfrac{\partial \mathbf{u}}{\partial \tau} + \varepsilon^4 m (\mathbf{u}\cdot\nabla)\mathbf{u} \right) = -\boldsymbol{\nabla} p, \quad \nabla \wedge \mathbf{u} = 0, \\ 1 + \dfrac{\gamma m}{\beta}\, p = \left(1 + \dfrac{m}{\alpha}\, \varrho \right)^\gamma, \end{cases} \tag{3.6}$$

$$\text{in the liquid:} \quad \begin{cases} \dfrac{\partial \varrho}{\partial \tau} + \mathrm{div}\mathbf{u} + m\varepsilon^4 \mathrm{div}(\rho \mathbf{u}) = 0, \\ \big(1 + \varepsilon^4 m\varrho \big) \left(\dfrac{\partial \mathbf{u}}{\partial \tau} + \varepsilon^4 m (\mathbf{u}\cdot\nabla)\mathbf{u} \right) = -\boldsymbol{\nabla} p, \quad \nabla \wedge \mathbf{u} = 0, \\ p = \varrho, \end{cases} \tag{3.7}$$

with initial conditions (i.c.) and boundary conditions at the bubble interface (b.c.)

$$\begin{cases} \text{i.c.} \quad p(\mathbf{x},0) = 0, \quad \varrho(\mathbf{x},0) = 0, \quad \mathbf{u}(\mathbf{x},0) = \mathbf{0}, \\ \text{b.c.} \quad p,\, \mathbf{u}\cdot\mathbf{n} \text{ are continuous and } \mathbf{u}\cdot\mathbf{n} = \dfrac{1}{\varepsilon^2} \dfrac{\mathsf{r}_{\rm eq}}{m}\, \dot{\mathsf{R}}. \end{cases} \tag{3.8}$$

4. Derivation of effective transmission conditions

The separation of the scales imposes that the asymptotic analysis is performed at three scales, the microscopic scale being that of a single bubble, the mesoscopic scale of the array where the bubbles are reduced to points and eventually the macroscopic scale of the waves, scale at which the whole screen is reduced to an interface $x_1 = 0$ (figure 2).

4.1. *Resolution at the microscopic scale - the scale of the bubble*

The microscopic scale is the scale corresponding to a zoom on a single bubble, which results in a bubble of radius constant and equal to unity in an infinite medium filled with liquid (the other bubbles are sent to infinity). This is obtained owing to the introduction of the coordinate

$$\mathbf{z} = \frac{1}{\mathsf{r}_{\rm eq} \mathsf{R}(\mathbf{x}',\tau)}\, \frac{\mathbf{x}}{\varepsilon^2},$$

where, following Caflisch *et al.* (1985*b*), the discrete version of the bubble radius R_i (see *e.g.* (2.4)) has been replaced by a continuous counterpart $\mathsf{R}(\mathbf{x}',\tau)$. Now, the differential

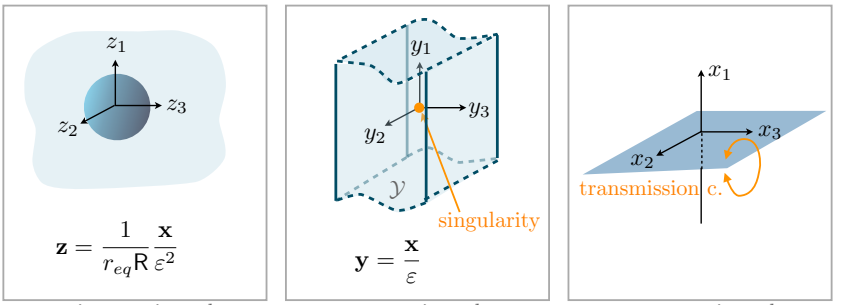

FIGURE 2. The problems at the three scales. At the microscopic scale, a single bubble lies in an infinite medium; at the mesoscopic scale, the bubble is reduced to a point singularity in a strip $\mathcal{Y}$ infinite along y_1 and periodic with respect to $\mathbf{y}' = (y_2, y_3)$; at the macroscopic scale, the bubbly screen is reduced to an interface across which transmission conditions apply.

operators in space and time read as

$$\boldsymbol{\nabla} \to \frac{1}{\mathsf{r}_{\rm eq}\mathsf{R}}\frac{\nabla_{\mathbf{z}}}{\varepsilon^2} + \nabla_{\mathbf{x}'} - \frac{\nabla_{\mathbf{x}'}\mathsf{R}}{\mathsf{R}}\,\mathbf{z}\cdot\nabla_{\mathbf{z}}\,, \quad \text{and} \quad \frac{\partial}{\partial\tau} \to \frac{\partial}{\partial\tau} - \frac{\dot{\mathsf{R}}}{\mathsf{R}}\,\mathbf{z}\cdot\nabla_{\mathbf{z}}\,. \tag{4.1}$$

We consider the following expansions of the solution in the gas

$$\begin{cases} \mathbf{u} = \dfrac{1}{\varepsilon^2}\hat{\mathbf{u}}_\mu^{-2}(\mathbf{z},\mathbf{x}',\tau) + \dfrac{1}{\varepsilon}\hat{\mathbf{u}}_\mu^{-1}(\mathbf{z},\mathbf{x}',\tau)\cdots, & p = \hat{p}_\mu^0(\mathbf{z},\mathbf{x}',\tau) + \varepsilon\hat{p}_\mu^1(\mathbf{z},\mathbf{x}',\tau) + \cdots, \\ \varrho = \hat{\varrho}_\mu^0(\mathbf{z},\mathbf{x}',\tau) + \varepsilon\hat{\varrho}_\mu^1(\mathbf{z},\mathbf{x}',\tau) + \cdots, & \mathsf{R} = \mathsf{R}^0(\mathbf{x}',\tau) + \varepsilon\mathsf{R}^1(\mathbf{x}',\tau) + \cdots, \end{cases} \tag{4.2}$$

and in the liquid (where $p = \varrho$)

$$\mathbf{u} = \frac{1}{\varepsilon^2}\mathbf{u}_\mu^{-2}(\mathbf{z},\mathbf{x}',\tau) + \frac{1}{\varepsilon}\mathbf{u}_\mu^{-1}(\mathbf{z},\mathbf{x}',\tau) + \cdots, \quad p = p_\mu^0(\mathbf{z},\mathbf{x}',\tau) + \varepsilon p_\mu^1(\mathbf{z},\mathbf{x}',\tau) + \cdots, \tag{4.3}$$

and the index μ stands for "microscopic".

4.1.1. *Resolution inside the bubble*

We shall establish that at the dominant order the pressure $\hat{p}_\mu^0$ and the mass density $\hat{\varrho}_\mu^0$ in a bubble are uniform, see (4.7)-(4.8). Plugging the expansions (4.2) in (3.6) along with (4.1), we get at the dominant order the following system

$$\begin{cases} \dfrac{\partial\hat{\varrho}_\mu^0}{\partial\tau} - \dfrac{\dot{\mathsf{R}}}{\mathsf{R}}\,\mathbf{z}\cdot\nabla_{\mathbf{z}}\,\hat{\varrho}_\mu^0 + \big(\alpha + m\hat{\varrho}_\mu^0\big)\dfrac{1}{\mathsf{r}_{\rm eq}\mathsf{R}^0}\mathrm{div}_{\mathbf{z}}\,\hat{\mathbf{u}}_\mu^{-2} + \dfrac{m}{\mathsf{r}_{\rm eq}\mathsf{R}^0}\nabla_{\mathbf{z}}\,\hat{\varrho}_\mu^0\cdot\hat{\mathbf{u}}_\mu^{-2} = 0, \\ \nabla_{\mathbf{z}}\,\hat{p}_\mu^0 = 0, \quad \nabla\wedge\hat{\mathbf{u}}_\mu^{-2} = 0, \\ 1 + \gamma\dfrac{m}{\beta}\hat{p}_\mu^0 = \Big(1 + \dfrac{m}{\alpha}\hat{\varrho}_\mu^0\Big)^\gamma, \end{cases} \tag{4.4}$$

with boundary and initial conditions

$$\begin{cases} \text{b.c. at } z = 1, \quad \hat{p}_\mu^0 = p_\mu^0, \quad \hat{\mathbf{u}}_\mu^{-2}\cdot\mathbf{e}_r = \dfrac{\mathsf{r}_{\rm eq}}{m}\,\dot{\mathsf{R}}^0, \\ \text{i.c. at } \tau = 0, \quad \hat{\mathbf{u}}_\mu^{-2} = \mathbf{0}, \quad \hat{p}_\mu^0 = \hat{\varrho}_\mu^0 = 0, \quad \mathsf{R}^0 = 1. \end{cases} \tag{4.5}$$

From (4.4), the pressure $\hat{p}_\mu^0$, hence the mass density $\hat{\varrho}_\mu^0$, are uniform inside a single bubble. It is worth noting that both still depend on time τ and on $\mathbf{x}'$. Next, $\hat{p}_\mu^0(\mathbf{x}',\tau)$ and $\hat{\varrho}_\mu^0(\mathbf{x}',\tau)$ can be expressed as a function of $\mathsf{R}^0(\mathbf{x}',\tau)$ only. To do so, we integrate the balance of

mass over the gas bubble (first equation in (4.4)) which leaves us with

$$\frac{4\pi}{3}\frac{\partial \hat{\varrho}_\mu^0}{\partial \tau} + \left(\alpha + m\hat{\varrho}_\mu^0\right)\frac{1}{\mathsf{r}_{\rm eq}\mathsf{R}^0}\int_{z=1}\hat{\mathbf{u}}_\mu^{-2}\cdot\mathbf{n}\,\mathrm{d}s = 0. \tag{4.6}$$

It is now sufficient to use from (4.5) (i) the boundary condition on $\hat{\mathbf{u}}_\mu^{-2}$ and (ii) the initial condition $\hat{\varrho}_\mu^0 = 0$ for $\mathsf{R}^0 = 1$, and we get after time integration that

$$\hat{\varrho}_\mu^0 = \frac{\alpha}{m}\left(\frac{1}{(\mathsf{R}^0)^3} - 1\right). \tag{4.7}$$

Eventually, making use of the equation of state (4.4), we also obtain the pressure

$$\hat{p}_\mu^0 = \frac{\beta}{\gamma m}\left(\frac{1}{(\mathsf{R}^0)^{3\gamma}} - 1\right). \tag{4.8}$$

Note that the velocity $\hat{\mathbf{u}}_\mu^{-2}$ is a subproduct of $\hat{\varrho}_\mu^0$ in (4.4), and it can be calculated once $\hat{\varrho}_\mu^0$, which is homogeneous with respect to $\mathbf{z}$, is known.

4.1.2. *Resolution in the liquid outside the bubble*

In the liquid, we proceed the same, plugging the expansions (4.3) in (3.6) along with (4.1). We get at the dominant order the following system

$$\begin{cases} \mathrm{div}_{\mathbf{z}}\,\mathbf{u}_\mu^{-2} = 0, \quad \nabla_{\mathbf{z}}\wedge\mathbf{u}_\mu^{-2} = 0, \\ \dfrac{\partial \mathbf{u}_\mu^{-2}}{\partial\tau} + \dfrac{m}{\mathsf{r}_{\rm eq}\mathsf{R}^0}(\mathbf{u}_\mu^{-2}\cdot\nabla_{\mathbf{z}})\mathbf{u}_\mu^{-2} - \dfrac{\dot{\mathsf{R}}^0}{\mathsf{R}^0}\,\mathbf{z}\cdot\nabla_{\mathbf{z}}\,\mathbf{u}_\mu^{-2} = -\dfrac{1}{\mathsf{r}_{\rm eq}\mathsf{R}^0}\nabla_{\mathbf{z}}\,p_\mu^0, \end{cases} \tag{4.9}$$

with boundary and initial conditions

$$\begin{cases} \text{b.c.} \quad \mathbf{u}_\mu^{-2}\cdot\mathbf{e}_r = \dfrac{\mathsf{r}_{\rm eq}}{m}\,\dot{\mathsf{R}}^0, \text{ at } z=1, \quad \lim\limits_{z\to+\infty} p_\mu^0(\mathbf{z},\mathbf{x}',\tau) = P^0(\mathbf{x}',\tau), \\ \text{i.c.} \quad \mathbf{u}_\mu^{-2} = \mathbf{0}, \quad p_\mu^0 = 0, \text{ at } \tau = 0. \end{cases} \tag{4.10}$$

The boundary condition for $z\to+\infty$ has been written introducing the field $P^0(\mathbf{x}',\tau)$; its meaning will appear later on. Also, we wrote the continuity of the normal velocity at $z=1$ (note that we should have written the continuity of the pressure, but for the time being, we do not need it). From (4.9), the flow is incompressible, hence it is associated to a velocity potential ϕ. Under the assumption that the bubble remains spherical when oscillates, the general form of the potential is $\phi = \frac{A}{z} + B$. It is now straightforward to solve (4.9): $\mathbf{u}_\mu^{-2} = \nabla_{\mathbf{z}}\,\phi$ is known from the boundary condition at $z=1$; next, p_μ^0 satisfies a modified Bernoulli equation of the form $\nabla_{\mathbf{z}}\,(p_\mu^0 + F(\dot{\mathsf{R}}^0,\ddot{\mathsf{R}}^0,z)) = 0$ (and F is obtained by integration), with the boundary condition at $z\to+\infty$. We get the velocity and the pressure fields $(\mathbf{u}_\mu^{-2}, p_\mu^0)$ as a function of R^0 and its time derivatives of the form

$$\mathbf{u}_\mu^{-2} = \frac{\mathsf{r}_{\rm eq}}{m}\dot{\mathsf{R}}^0\,\frac{\mathbf{e}_r}{z^2}, \qquad p_\mu^0 = P^0 + \frac{\mathsf{r}_{\rm eq}^2}{m}\left(\frac{\mathsf{R}^0\ddot{\mathsf{R}}^0 + 2(\dot{\mathsf{R}}^0)^2}{z} - \frac{(\dot{\mathsf{R}}^0)^2}{2z^4}\right). \tag{4.11}$$

4.1.3. *An equation of the Rayleigh-Plesset's type*

At this stage, once $\mathsf{R}^0(\mathbf{x}',\tau)$ is known, the solution inside the bubble is known from (4.7)-(4.8), and the solution inside the liquid is known up to a function $P^0(\mathbf{x}',\tau)$ from (4.11). As an intermediate result, R^0 satisfies a continuous version of the Rayleigh-Plesset equation, being parametrized by $\mathbf{x}'$. Indeed, using the continuity of the pressure across

the bubble boundary $p^0_\mu = \hat{p}^0_\mu$ at $z = 1$, and reporting $z = 1$ in (4.11), we get that $\mathsf{R} = \mathsf{R}^0$ is solution of

$$\mathsf{R}\ddot{\mathsf{R}} + \frac{3}{2}\dot{\mathsf{R}}^2 = \frac{m}{\mathsf{r}^2_{\rm eq}}\left(\hat{p}^0_\mu - P^0\right), \tag{4.12}$$

where $\left(\hat{p}^0_\mu - P^0\right)$ is the difference of the pressures inside a bubble and far from it. This holds for all bubbles whose positions are parametrized by $\mathbf{x}'$ (and both $\hat{p}^0_\mu$ and P^0 depend on $\mathbf{x}'$). Eventually, since $\hat{p}^0_\mu$ is known in (4.8), we see that R^0 satisfies a differential equation with a source P^0 only, namely R^0 is solution of

$$\mathsf{R}\ddot{\mathsf{R}} + \frac{3}{2}\dot{\mathsf{R}}^2 - \frac{\beta}{\gamma \mathsf{r}^2_{\rm eq}}\frac{1}{\mathsf{R}^{3\gamma}} = -\frac{1}{\mathsf{r}^2_{\rm eq}}\left(\frac{\beta}{\gamma} + mP^0\right), \tag{4.13}$$

and expectedly $P^0 = 0$ corresponds to the equilibrium (with $\mathsf{R} = \mathsf{R}^0 = 1$ and $\hat{p}^0_\mu = 0$ solution of (4.9)-(4.10)).

4.2. *Resolution at the mesoscopic scale - the scale of the array spacing*

From the preceding section, we know that the solution at the microscopic scale is known once $P^0(\mathbf{x}', \tau)$ is known, and P^0 will be provided by the problem at the mesoscopic scale. This scale corresponds to that of the array spacing which, by construction, is intermediate between the bubble size and the typical wavelength. The zoom on this scale is performed owing to the new coordinate $\mathbf{y}$ defined by $\mathbf{y} = \dfrac{\mathbf{x}}{\varepsilon}$, with the associated differential operator

$$\boldsymbol{\nabla} \to \frac{1}{\varepsilon}\nabla_{\mathbf{y}} + \nabla_{\mathbf{x}'}\,. \tag{4.14}$$

The problem is defined in a strip $\mathcal{Y}$ infinite along y_1 (the direction perpendicular to the array) and bounded in $\mathbf{y}' = (y_2, y_3) \in \mathsf{Y}$, with $\mathsf{Y} = (-1/2, 1/2)^2$ (hence $\mathcal{Y} = \mathbb{R} \times \mathsf{Y}$). We assume the following expansions

$$\begin{cases} \mathbf{u} = \mathbf{u}^0_{\rm m}(\mathbf{y}, \mathbf{x}', \tau) + \varepsilon \mathbf{u}^1_{\rm m}(\mathbf{y}, \mathbf{x}', \tau) + \cdots, \\ \\ p = p^0_{\rm m}(\mathbf{y}, \mathbf{x}', \tau) + \varepsilon p^1_{\rm m}(\mathbf{y}, \mathbf{x}', \tau) + \cdots, \quad \varrho = \varrho^0_{\rm m}(\mathbf{y}, \mathbf{x}', \tau) + \varepsilon \varrho^1_{\rm m}(\mathbf{y}, \mathbf{x}', \tau) + \cdots, \end{cases} \tag{4.15}$$

with each term $(\mathbf{u}^i_{\rm m}, p^i_{\rm m}, \varrho^i_{\rm m})$, $i = 0, 1, \cdots$, in the expansions being periodic functions of $\mathbf{y}' \in \mathsf{Y}$, and where the index m stands for "mesoscopic".

4.2.1. *Matching conditions*

The matching conditions tell us that the solution of the microscopic problem has to coincide with that of the mesoscopic problem in some intermediate region, when $z \to \infty$ and $y \to 0$. With $y = O(x/\varepsilon)$ and $z = O(x/\varepsilon^2)$, this intermediate region is typically at the distance $\varepsilon\sqrt{\varepsilon}$ of the bubble, in $\mathbf{x}$ coordinate; hence, approaching this region with $z \sim 1/\sqrt{\varepsilon} \to +\infty$ corresponds to $y \sim \sqrt{\varepsilon} \to 0$. The resulting matching conditions are obtained by matching, for $y \to 0$, the expansions (4.2), with $\mathbf{z} = \mathbf{y}/(\mathsf{r}_{\rm eq}\mathsf{R}\varepsilon)$, and the expansions (4.15). For the pressure, only the matching condition at the order 0 is needed, namely

$$p^0_{\rm m}(\mathbf{y}, \mathbf{x}', \tau) + \cdots \underset{y\to 0}{\sim} p^0_\mu\left(\frac{\mathbf{y}}{\mathsf{r}_{\rm eq}\varepsilon\mathsf{R}}, \mathbf{x}', \tau\right) + \cdots \Rightarrow p^0_{\rm m}(\mathbf{0}, \mathbf{x}', \tau) = \lim_{z\to+\infty} p^0_\mu(\mathbf{z}, \mathbf{x}', \tau) = P^0(\mathbf{x}', \tau). \tag{4.16}$$

The pressure field P^0 introduced in (4.10) corresponds to the pressure field $p^0_{\rm m}$ at $y = 0$ where the bubble, reduced to a point, is located. Next, the matching condition for the

velocity reads as

$$\mathbf{u}_{\mathrm{m}}^0(\mathbf{y},\mathbf{x}',\tau)+\cdots \underset{y\to 0}{\sim} \frac{1}{\varepsilon^2}\mathbf{u}_\mu^{-2}\left(\frac{\mathbf{y}}{\mathsf{r}_{\mathrm{eq}}\varepsilon\mathsf{R}},\mathbf{x}',\tau\right)+\cdots, \Rightarrow \mathbf{u}_{\mathrm{m}}^0 \underset{y\to 0}{\sim} \frac{\mathsf{r}_{\mathrm{eq}}^3}{m}\,(\mathsf{R}^0)^2\dot{\mathsf{R}}^0\,\frac{\mathbf{e}_r}{y^2}. \quad (4.17)$$

We used $\mathbf{u}_\mu^{-2}$ in (4.11), and we assumed that the terms $\mathbf{u}_\mu^n$, when increasing $n > -2$, decrease faster than $\mathbf{u}_\mu^{-2} \propto 1/z^2$; note that this is consistent with non diverging mass flux through a sphere. This is the main result provided by the mesoscopic scale: the term $\mathbf{u}_{\mathrm{m}}^0$ is singular at the origin, and it encapsulates the effect of the oscillating bubble point (if $\dot{\mathsf{R}}^0 = 0$, the bubble is not seen and $\mathbf{u}_{\mathrm{m}}^0$ is regular).

4.2.2. *The mesoscopic problem up to* $\mathbf{u}_{\mathrm{m}}^0$

To get the problem at the dominant order, we inject (4.15) in (3.6) along with (4.14). As a first result at the dominant order, we get that $\nabla_{\mathbf{y}}\, p_{\mathrm{m}}^0 = \mathbf{0}$, hence p_{m}^0 does not depend on $\mathbf{y}$, and from (4.16), we obtain that

$$p_{\mathrm{m}}^0(\mathbf{y},\mathbf{x}',\tau) = P^0(\mathbf{x}',\tau). \quad (4.18)$$

It follows that the problem at the dominant order is set on $(\mathbf{u}_{\mathrm{m}}^0, p_{\mathrm{m}}^1)$ and it reads as

$$\mathrm{div}_{\mathbf{y}}\,\mathbf{u}_{\mathrm{m}}^0 = \mathbf{0}, \quad \nabla\wedge\mathbf{u}_{\mathrm{m}}^0 = \mathbf{0}, \quad \frac{\partial\mathbf{u}_{\mathrm{m}}^0}{\partial\tau} = -\nabla_{\mathbf{x}'}\,P^0(\mathbf{x}',\tau) - \nabla_{\mathbf{y}}\,p_{\mathrm{m}}^1, \quad (4.19)$$

with boundary and initial conditions

$$\begin{cases} \text{b.c.} & \lim\limits_{y_1\to\pm\infty}\mathbf{u}_{\mathrm{m}}^0 = \mathbf{U}^{0\pm}(\mathbf{x}',t), \quad p_{\mathrm{m}}^1, \mathbf{u}_{\mathrm{m}}^0 \text{ periodic on } \partial\mathsf{Y}, \\ \text{i.c.} & p_{\mathrm{m}}^1 = 0,\ \mathbf{u}_{\mathrm{m}}^0 = \mathbf{0} \text{ at } \tau = 0, \end{cases} \quad (4.20)$$

and $\mathbf{u}_{\mathrm{m}}^0$ is singular at $y = 0$ with the form of the singularity given in (4.17). At the mesoscopic scale, we have three unknown fields: P^0 that we reach back from the microscopic scale (see Eq. (4.10)) and $\mathbf{U}^{0\pm}$ that we introduce in (4.20). These fields will be used to derive the transmission conditions at the macroscopic scale.

4.3. *Derivation of the effective transmission conditions*

We now dive into the problem at the macroscopic scale, where only the coordinate $\mathbf{x}$ is needed, and we consider the following expansions

$$\mathbf{u} = \mathbf{u}^0(\mathbf{x},\tau)+\varepsilon\mathbf{u}^1(\mathbf{x},\tau)+\cdots, p = p^0(\mathbf{x},\tau)+\varepsilon p^1(\mathbf{x},\tau)+\cdots, \varrho = \varrho^0(\mathbf{x},\tau)+\varepsilon\varrho^1(\mathbf{x},\tau)+\cdots. \quad (4.21)$$

At this scale, the bubble screen has been reduced to an interface but there are missing boundary conditions when $x_1 \to 0^\pm$. These are the conditions that we are looking for and they will be provided by matching the solutions of the mesoscopic and macroscopic problems. The intermediate region where both solutions are valid corresponds to $x_1 \sim \sqrt{\varepsilon} \to 0^\pm$, hence $y_1 \sim 1/\sqrt{\varepsilon} \to \pm\infty$. At the dominant order, we get

$$\begin{cases} p^0(0^\pm,\mathbf{x}',\tau) = \lim\limits_{y_1\to\pm\infty} p_{\mathrm{m}}^0(\mathbf{y},\mathbf{x}',\tau) = P^0(\mathbf{x}',\tau), \\ \mathbf{u}^0(0^\pm,\mathbf{x}',\tau) = \lim\limits_{y_1\to\pm\infty} \mathbf{u}_{\mathrm{m}}^0(\mathbf{y},\mathbf{x}',\tau) = \mathbf{U}^{0\pm}(\mathbf{x}',\tau), \end{cases} \quad (4.22)$$

where we used (4.18) and (4.20). Eventually, from (3.6) at the dominant order, $(p^0, \mathbf{u}^0)$ satisfy the linearized Euler equation in an irrotational flow

$$\frac{\partial p^0}{\partial\tau} + \mathrm{div}_{\mathbf{x}}\mathbf{u}^0 = 0, \quad \frac{\partial\mathbf{u}^0}{\partial\tau} = -\nabla_{\mathbf{x}}p^0, \quad \nabla\wedge\mathbf{u}^0 = 0, \quad (4.23)$$

with the boundary conditions (4.22) and the initial conditions $p^0(\mathbf{x},0) = 0$, $\mathbf{u}^0(\mathbf{x},0) = \mathbf{0}$.

From (4.22), the pressure p^0 is found to be continuous at $x_1 = 0$, hence

$$[\![p^0]\!] = 0. \tag{4.24}$$

This is not the case for the normal velocity, and to show this result, we have to come back to the problem satisfied by $\mathbf{u}_{\rm m}^0$. The equation of incompressibility, $\mathrm{div}_{\mathbf{y}}\, \mathbf{u}_{\rm m}^0 = 0$ in (4.19), is integrated in the domain $\mathcal{Y}$ minus a ball B_r of radius r (in order to avoid the singularity of $\mathbf{u}_{\rm m}^0$). Using the boundary conditions in (4.20) and the singular behavior of $\mathbf{u}_{\rm m}^0$ in (4.17), we get

$$\mathbf{0} = \int_{\mathcal{Y}/B_r} \mathrm{div}_{\mathbf{y}}\, \mathbf{u}_{\rm m}^0\, d\mathbf{y} = u_1^0(0^+, \mathbf{x}', \tau) - u_1^0(0^-, \mathbf{x}', \tau) - \int_{\partial B_r} \frac{\mathsf{r}_{\rm eq}^3}{m} \frac{(\mathsf{R}^0)^2 \dot{\mathsf{R}}^0}{y^2} d\mathbf{y}. \tag{4.25}$$

The integral over ∂B_r gives a finite but non zero contribution (independent of r), and eventually a non trivial transmission condition for u_1^0 involving $[\![u_1^0]\!] \equiv u_1^0(0^+, \mathbf{x}', t) - u_1^0(0^-, \mathbf{x}', t)$ of the form

$$[\![u_1^0]\!] = \frac{4\pi \mathsf{r}_{\rm eq}^3}{m} (\mathsf{R}^0)^2 \dot{\mathsf{R}}^0. \tag{4.26}$$

5. Discussion on the effective screen problem

5.1. *The final effective screen model*

Once coming back to the fields with dimension, the effective problem, from (4.13), (4.23),(4.24) and (4.26), applies in the liquid where the bubbly screen has disappeared. In the liquid, $(P, \mathbf{U})$ satisfy

$$\frac{\partial P}{\partial t} + \rho_\ell c_\ell^2 \mathrm{div}\mathbf{U} = 0, \quad \rho_\ell \frac{\partial \mathbf{U}}{\partial t} = -\boldsymbol{\nabla} P, \quad \nabla \wedge \mathbf{U} = 0, \tag{5.1}$$

with the initial conditions and radiation conditions being the same as in the actual problem. The effect of the bubbly screen on the plane Γ ($X_1 = 0$) is reduced to effective transmission conditions which read as

$$\begin{cases} [\![P]\!] = 0, \quad [\![U_1]\!] = \dfrac{4\pi R^2}{h^2}\, \dot{R}, \\ \\ \rho_\ell \left(R\ddot{R} + \dfrac{3}{2}\dot{R}^2 \right) + \dfrac{\rho_{\rm g} c_{\rm g}^2}{\gamma} \left(1 - \left(\dfrac{R_{\rm eq}}{R} \right)^{3\gamma} \right) = -P_{|X_1 = 0}, \end{cases} \tag{5.2}$$

with $R(\mathbf{X}', t)$ and $P(0, t) = P(0, \mathbf{X}', t)$ (and remember that $P_{\rm eq} = \rho_{\rm g} c_{\rm g}^2/\gamma$). As previously said, a similar model has been derived in Miksis & Ting (1989) starting from the model of Caflisch *et al.* (1985*b*) valid for a thick bubbly medium and reducing its thickness $h_{\rm l}$ up to h. The natural parameter measuring the spacing in the bubbly liquid and the volume fraction n of bubbles and it turns out that the model is identical to ours if we set $h_{\rm l} = h$; specifically our parameter $4\pi/h^2$ in (5.2) reads as $3nh_{\rm l}/R_{\rm eq}^3$ in this reference. The same applies if we consider a thin layer made of N bubbles; by linearity of the jump condition, it is sufficient to use in (5.2) $4\pi/h^2$ by $4N\pi/h^2$, hence to set $h_{\rm l} = Nh$ in Miksis & Ting (1989). It may appear natural that the two models coincide but this is not the rule; conducting the calculations using firstly homogenization technique of thick media then asymptotic tools in the limit of vanishing thickness of the resulting effective medium does not always conduce to the right solution, see *e.g.* Marigo & Maurel (2016). Nevertheless, it is a good news that the two models coincide in the present case and an exhaustive numerical study of the range of validity of the interface model for

increasing layer thickness can be found in Miksis & Ting (1989). Eventually, we point out an incidental difference of our result in non dimensional form (4.26) with respect to Eq. (31) in Miksis & Ting (1989). The non dimensional parameter κ measuring the strength of the interaction between the screen and the acoustic wave reads, from (4.26) along with (3.5), as

$$\kappa = 4\pi \left(\frac{\omega R_{\rm eq}}{c_\ell}\right)\left(\frac{R_{\rm eq}}{h}\right)^2 \frac{1}{Ma}, \tag{5.3}$$

while the dependence on the Mach number is missing in Miksis & Ting (1989) and this is attributable to the fact that the pressure fluctuations varies as the Mach number and not as the pressure at equilibrium, see (3.3). This allows us to anticipate that larger effect of the bubbly screen (large κ) are expected when decreasing the spacing h and Ma, and this will be illustrated in the §6.

5.2. *Equation of energy conservation*

The resolution of the effective model (5.1)-(5.2) requires to account for the transmission conditions which encapsulates the coupling of the screen with the fluid. To understand the resulting exchange of energy, we write the equation of energy conservation. In any bounded domain Ω, this equation reads as

$$\frac{d}{dt}\mathcal{E} + \Phi = 0, \quad \text{with } \mathcal{E} = \frac{1}{2}\int_\Omega \left(\frac{P^2}{\rho_\ell c_\ell^2} + \rho_\ell U^2\right) \mathrm{d}\mathbf{X}, \tag{5.4}$$

with $\mathcal{E}$ the acoustic energy and $\Phi = \int_{\partial\Omega} P\,\mathbf{U}\cdot\mathbf{n}\,\mathrm{d}S$ the flux of the Poynting vector. The boundary $\partial\Omega$ involves the usual boundaries crossed by ingoing and outgoing waves. However, because Γ is a surface of discontinuity, Φ has a contribution $\Phi_\Gamma = -\int_\Gamma P\,[\![U_1]\!]\,d\mathbf{X}'$ that we have to specify. It is easy to see that

$$\Phi_\Gamma = \frac{d}{dt}\mathcal{E}_\Gamma, \qquad \text{with } \mathcal{E}_\Gamma = \int_\Gamma (\mathcal{E}_{\rm c} + \mathcal{E}_{\rm p})\,\mathrm{d}\mathbf{X}', \tag{5.5}$$

with

$$\mathcal{E}_{\rm c} = 2\pi\rho_\ell \left(\frac{R^{\frac{3}{2}}\dot{R}}{h}\right)^2, \quad \mathcal{E}_{\rm p} = \frac{M_{\rm g} c_{\rm g}^2}{\gamma\, h^2}\left[-\frac{\gamma}{\gamma-1} + \left(\frac{R}{R_{\rm eq}}\right)^3 + \frac{1}{\gamma-1}\left(\frac{R_{\rm eq}}{R}\right)^{3(\gamma-1)}\right], \tag{5.6}$$

where $M_{\rm g} = \frac{4\pi}{3}\rho_{\rm g} R_{\rm eq}^3$ is the constant mass of a bubble †. Next, $\mathcal{E}_\Gamma$ is the effective energy by unit cell supported by the effective screen Γ, with $\mathcal{E}_{\rm c}$ and $\mathcal{E}_{\rm p}$ the kinetic and potential energies respectively.

It is worth noting that the effective energy of the screen is positive, with $\mathcal{E}_{\rm c} = \mathcal{E}_{\rm p} = 0$ at the equilibrium and $\mathcal{E}_{\rm c} > 0$, $\mathcal{E}_{\rm p} > 0$ otherwise. This is not incidental since it guaranties that the effective problem is written in a suitable form for numerical implementation. Loosely speaking, this ensures that, in the absence of fluxes exchanged with the exterior of Ω, the total energy $(\mathcal{E} + \mathcal{E}_\Gamma)$ is conserved in time, without possible time variations of $\mathcal{E}$ compensated by opposite time variations of $\mathcal{E}_\Gamma$ which would foster numerical (and unphysical) instabilities, see *e.g.* Lombard *et al.* (2017).

5.3. *Analysis of the radiative damping in a one-dimensional problem*

In the Rayleigh-Plesset equation (5.2), the forcing term for the non-linear resonator is the acoustic pressure $P_{|X_1=0}$, which does not coincide with the initial pulse $P_{{\rm in}|X_1=0}$.

† Note that, to derive (5.6), we used notably that $\frac{d}{dt}\left(R^{\frac{3}{2}}\dot{R}\right)^2 = 2R^2\dot{R}\left(R\ddot{R} + \frac{3}{2}\dot{R}^2\right)$.

To understand the underlying difference, we shall consider a one-dimensional problem, which means that a right-going (respectively left-going) wave in the fluid is described by a function $F(t - X_1/c_\ell)$ (respectively $F(t + X_1/c_\ell)$), from (5.1). Now, setting $\eta = (R_{\rm eq}/h)^2 \ll 1$, we use the expansions $P = P^0 + \eta\, P^1 + \dots$ and $R = R^0 + \eta\, R^1 + \dots$ in (5.2) to get that

$$[\![P^0]\!] = [\![P^1]\!] = 0, \quad \text{and } [\![U_1^0]\!] = 0, [\![U_1^1]\!] = 4\pi \left(\frac{R^0}{R_{\rm eq}}\right)^2 \dot{R}^0. \tag{5.7}$$

At the dominant order, the screen is not seen hence the incident pulse propagates without deformation which reads as $P^0(X_1, t) = P_{\rm in}(t - X_1/c_\ell)$, where $P_{\rm in}(-X_1/c_\ell)$ is the pulse imposed at $t = 0$. This also means that P^1 corresponds to scattered wave trains, and as such it can be written in the form $P^1(X_1, t) = F(t \pm X_1/c_l)$ for right and left-going waves, with the continuity of P^1 at the screen. It follows that $U^1(0^\pm, t) = \pm F(t)/(\rho_\ell c_\ell)$, and the jump condition (5.7) on U_1 leaves us with $F(t) = 2\pi\rho_\ell c_\ell \left(\frac{R^0}{R_{\rm eq}}\right)^2 \dot{R}^0 = P^1(0, t)$. It is now sufficient to come back to $(R^0 + \eta\, R^1)$ and $(P^0 + \eta\, P^1)$ which admit the same expansion as R and P up to $O(\eta^2)$ to get an approximate expression of $P(0, t)$ of the form

$$P(0, t) \simeq P_{\rm in}(X_1, t) + 2\pi\rho_\ell c_\ell \frac{R^2}{h^2}\dot{R}, \tag{5.8}$$

and a modified Rayleigh-Plesset equation for R valid for small $(R_{\rm eq}/h)$ of the form

$$\rho_\ell \left(R\ddot{R} + \frac{3}{2}\dot{R}^2\right) - \frac{\rho_{\rm g} c_{\rm g}^2}{\gamma}\left(\frac{R_{\rm eq}}{R}\right)^{3\gamma} + \frac{2\pi\rho_\ell c_\ell}{h^2}\, R^2\dot{R} = -P_{{\rm in}|X_1=0}. \tag{5.9}$$

By inspection of the above expression compared to (5.2), the equation of the non-linear oscillator contains a term of loss through $R^2\dot{R}$ which was primarily encapsulated in the term of pressure $P_{|X_1=0}$; these losses corresponds to the radiative damping and are responsible for the interaction between the bubbles and the surrounding fluid. To be more explicit, in the linear regime, (5.9) takes the form

$$\rho_\ell R_{\rm eq}\left(\ddot{r} + \frac{2}{\tau}\,\dot{r} + \omega_{\rm M}^2 r\right) = -P_{{\rm in}|X_1=0}, \tag{5.10}$$

with

$$\tau = \frac{1}{\pi}\frac{R_{\rm eq}}{c_\ell}\left(\frac{h}{R_{\rm eq}}\right)^2, \quad \omega_{\rm M}\tau = \frac{\sqrt{3}}{\pi}\sqrt{\frac{\rho_{\rm g} c_{\rm g}^2}{\rho_\ell c_\ell^2}}\left(\frac{h}{R_{\rm eq}}\right)^2. \tag{5.11}$$

For the screen, the radiative damping plays the same role as the viscosity which would produce $(4\nu_{\rm eff}/R_{\rm eq}^2)\ \dot{r}$, with $\nu_{\rm eff} = \frac{\pi}{2}\, c_\ell \frac{R_{\rm eq}^3}{h^2}$. It is worth noting that $\omega_{\rm M}\tau = O(1)$ in our model (by construction), hence it covers the transition from over- to under-damped oscillations.

6. Numerical results

In this section, we inspect the characteristics of the effective model in the linear and non linear regimes. We set the physical constants as follow: $\rho_l = 10^3$ Kg.m^{-3}, $c_\ell = 1\ 500$ m.s^{-1}, $\gamma = 1.4$, $R_{\rm eq} = 10^{-5}$ m $P_{\rm eq} = 0.225$ atm. and we shall consider different value of the array spacing $h/R_{\rm eq}$.

In the linear regime, the Minnaert resonance frequency is $\omega_{\rm M} = \sqrt{3\gamma P_{\rm eq}/(\rho_\ell R_{\rm eq}^2)} \simeq 10^6$

Hz. Following Doc *et al.* (2016), we consider an initial Gaussian pulse of the form

$$P_{\rm in}(X_1, t_{\rm ini}) = \Delta P \, e^{-(X_1 - X_{\rm ini})^2/\sigma^2}, \tag{6.1}$$

With a wavelength at the resonance $\lambda_{\rm M} = 10^{-2}$ m, we set the spatial extension of the pulse $\sigma = \lambda_{\rm M}/10 = 10^{-3}$ m. To the characteristic lengths $\lambda_{\rm M}$ and σ, we associate the characteristic times $T = \lambda_{\rm M}/c_\ell \sim 6.10^{-6}$ s the period of the Minnaert resonance and $T_\sigma = T/10$ s the duration of the pulse. In our computations, the 1D domain is set in $X_1 \in (-100\sigma, 100\sigma)$ m. The pulse is sent at $t_{\rm ini} = -30T_\sigma$ with $X_{\rm ini} = -30\sigma$ m, hence it reaches the interface located at $X_1 = 0$ at time $t = 0$.

Making use of the above numerical values, the Mach number and the parameter κ measuring the strength of the interaction, Eq. (5.3), are given by

$$Ma = 10^{-5}\,\frac{\Delta P}{P_{\rm eq}}, \quad \kappa \simeq 10^4\,\frac{(R_{\rm eq}/h)^2}{\Delta P/P_{\rm eq}}, \tag{6.2}$$

hence in our computations, the effect of the screen on the spacing h and on the non-linearities (by means of the Mach number) will be inspected.

6.1. *Validation of the numerical implementation*

In this section, we consider $\Delta P/P_{\rm eq} = 10^{-3}$ for which we expect weak amplitude of the bubble oscillations, and we terme this regime the linear regime (the propagation of the acoustic acoustic wave train in the fluid is linear in any cases, from (5.1)). The array spacing is set to $h = 20R_{\rm eq}$ hence the low frequency regime measured by $\varepsilon = \frac{\omega_{\rm M}}{c_\ell} h$ is $\varepsilon = 0.13$.

The figure 3 shows a typical time series of the wave train $P(X_1, t)$ during propagation; the interaction of the incident pulse with the screen is visible by means of the reflected and transmitted pulses for $t > 0$. The Fourier transform of the reflected signal allows to extract the reflection coefficient against ω. The result reported in figure 4(a) is consistent with the analytical form of R explicit in the linear regime, see (A 3). Eventually, figure 4(b) show the normalized reflected $E_{\rm R}(t)$ and transmitted $E_{\rm T}(t)$ energies computed from (5.4) in the fluid for $X_1 < 0$ and $X_1 > 0$ respectively; the normalization is done with respect to the energy of the initial pulse. We also report the normalized energy of the bubbles $E_{\rm B}$ from (5.6). This representation supports two informations of different nature: (i) the numerical implementation is consistent with the conservation of the energy with $E_{\rm tot}(t)$ the sum of the 3 energy being close to 1, (ii) the bubbly screen conserves energy over a time much larger than the pulse duration due to its oscillation, and this will be commented in the following.

6.2. *Influence of the array spacing*

We now focus on the influence of the array spacing h. The figure 5 shows the forms of the pressure signal $P(0, t)$ and the bubble radius $R(t)$ for increasing spacing $h/R_{\rm eq}$ from 10 to 640 in a regime of linear oscillations ($\Delta P/P_{\rm eq} = 10^{-3}$) and in a regime of non-linear oscillations ($\Delta P/P_{\rm eq} = 15$).

Let us start by analyzing the linear regime. For our Gaussian initial pulse, and making use of (5.10), it is easy to see that $R(t)$ is roughly given by

$$R(t) \simeq R_{\rm eq} + \sqrt{\pi}\sigma\,\frac{\Delta P}{\rho_\ell c_\ell R_{\rm eq}\omega_{\rm S}}\,\sin(\omega_{\rm S} t)\, e^{-t/\tau}, \tag{6.3}$$

with $\omega_{\rm S} = \sqrt{\omega_{\rm M}^2 - 1/\tau^2}$, and τ increases with increasing $(h/R_{\rm eq})$, from (5.11). For very

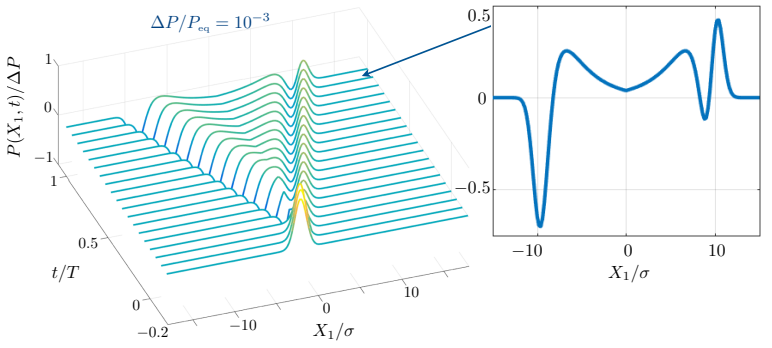

FIGURE 3. Propagation of an initial Gaussian pulse in the linear regime of oscillation, $P(X_1, t)$ for $h/R_{\rm eq} = 20$. The inset shows a profile $P(X_1, T)$ with $T = 10T_\sigma$.

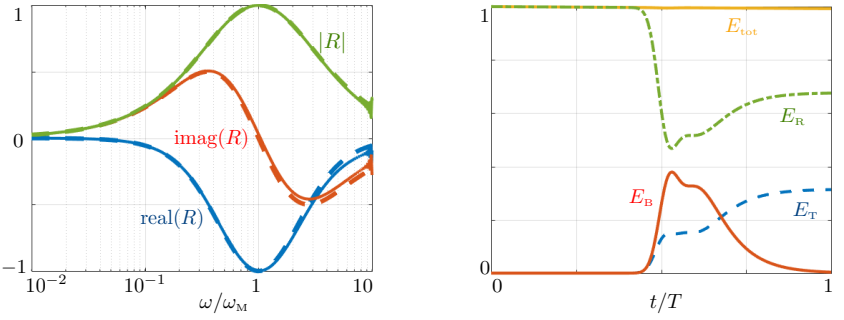

(a) (b)

FIGURE 4. (a) Reflection coefficient R computed by means of the Fourier transform of the reflected wave train for $t > T$ (plain lines) and from the linear analysis (A 3) (dashed lines). $h/R_{\rm eq} = 20$ and $\Delta P/P_{\rm eq} = 10^{-3}$. (b) Temporal evolution of the energies (normalized with the energy of the incident pulse). $E_{\rm R}$ and $E_{\rm T}$ are the energies in the fluid, computed for $X_1 < 0$ and $X_1 > 0$, from (5.4), and $E_{\rm B}$ is energy of the bubbly screen from (5.6); $E_{\rm tot} = E_{\rm R} + E_{\rm T} + E_{\rm B}$.

large spacings the bubbles within the screen oscillate at the Minnaert frequency which is intuitive since they are expected to behave as if they were in free space in this limit; from (6.3), the oscillation amplitude is simply proportional to ΔP with

$$\frac{R}{R_{\rm eq}} - 1 \simeq \frac{\sigma \Delta P}{\rho_\ell c_\ell R_{\rm eq}^2 \omega_{\rm M}}. \tag{6.4}$$

Bringing them closer produces weakened oscillations up to an overdamped regime, visible for $h/R_{\rm eq} = 10$ and 20 (in the present case, $\omega_{\rm M}\tau \simeq \left(\frac{h/R_{\rm eq}}{22}\right)^2$). The same scenario is observed in the non linear regime, with a saturation of the oscillation amplitude compared to the linear expectation (6.4).

Both in the linear and non linear regimes, the form of $P(0, t)$ appears to satisfy the estimate in (5.8). Specifically, $P(0, t)$ coincides merely with the incident pulse if $h/R_{\rm eq} \gg \sqrt{\sigma/R_{\rm eq}} = 10$. In this case, the pressure fluctuations generated by the bubbles when oscillate are of amplitude as small as $(R_{\rm eq}\sigma/h^2)\Delta P$ in the linear regime and even smaller in the non-linear regime. This is illustrated in figure 6 where we report a typical profile of the pressure fluctuations emitted by the screen after the initial pulse has passed through it. It is worth noting that even when the bubbles oscillate in a non-linear regime, the

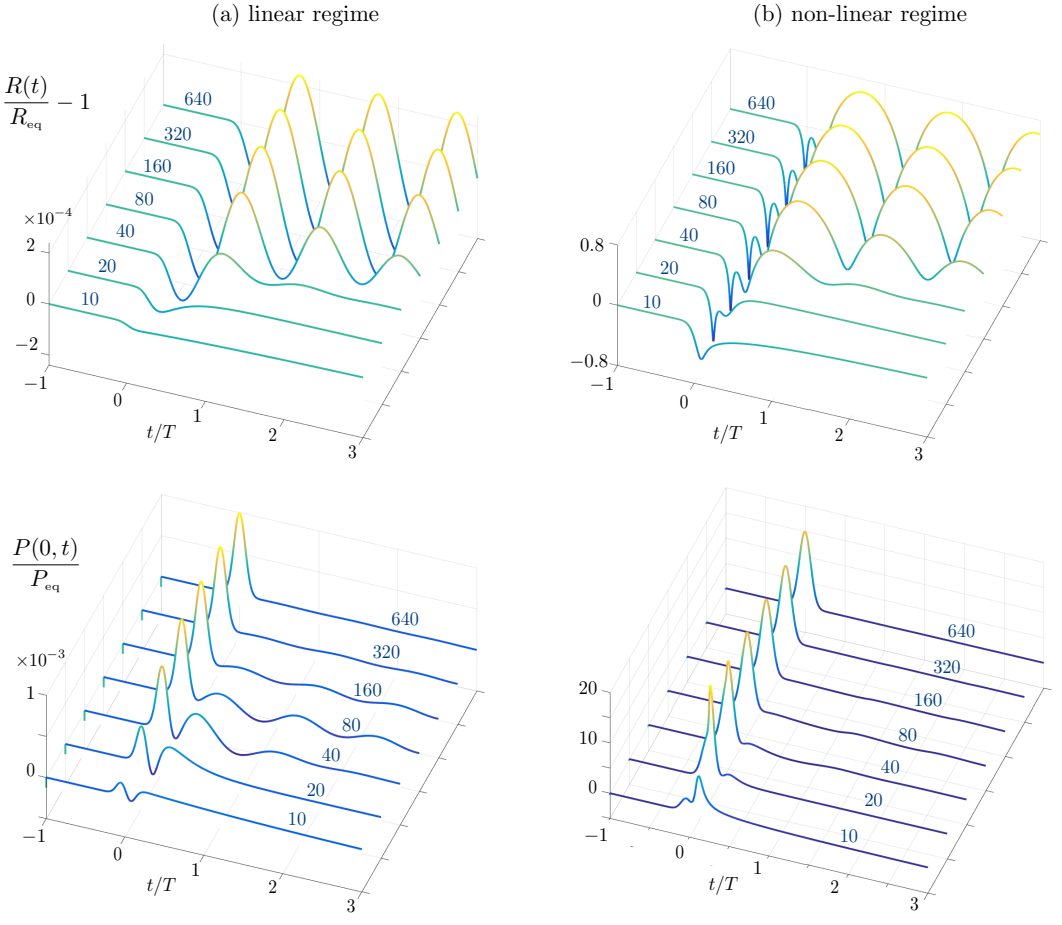

FIGURE 5. Influence of the array spacing $h/R_{eq} = 10$, 20, 40, 80, 160 320 and 640 (a) in the linear regime, $\Delta P/P_{eq} = 10^{-3}$ and (b) in the non-linear regime, $\Delta P/P_{eq} = 15$.

resulting pressure fluctuations propagate linearly in the fluid, on the right and on the left far from the screen.

To summarize, the effect of the bubbly screen on the acoustic wave train decreases when the spacing between the bubbles increases even though the ability of acoustic fluctuations to excite them increases. Physically, this is attributable to the fact that the bubbles behaving as almost perfect resonators with low leakage do not need much energy to oscillate during long time. Hence, in the limit of large h/R_{eq} the screen becomes invisible for the acoustic waves, see figure 7 where we report the transmitted and reflected energies at large time (once the bubbles have released their energy).

6.3. *Influence of the non-linearities*

Here, we shall inspect the influence of the non-linearity, and to anticipate we shall confirm what we have seen in the previous section, namely that higher non-linearities prevent from large effects of the bubbly screen on acoustic waves. The figure 8 reports time series of the acoustic wave trains during propagation for $h/R_{eq} = 20$ and increasing

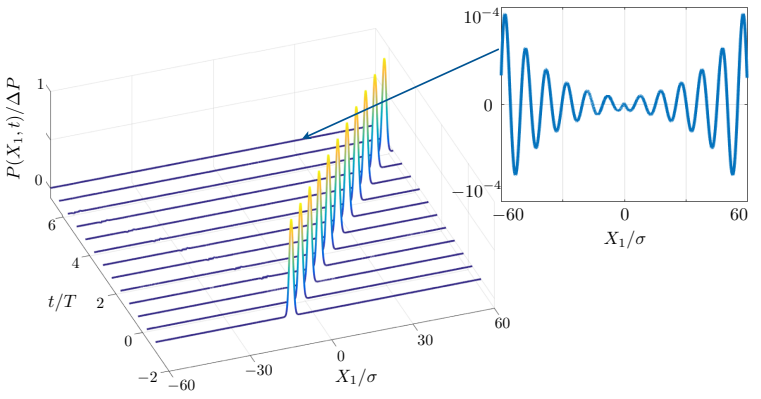

FIGURE 6. Propagation of an initial Gaussian pulse in the non-linear regime of oscillation for large array spacing $h/R_{\mathrm{eq}} = 80$; same representation as in figure 3. The inset shows a profile of the pressure wave train emitted by the bubbly screen after the initial pulse has passed through it. Although the bubbles oscillate in a non-linear regime regime, the resulting wave train propagation is linear in the fluid.

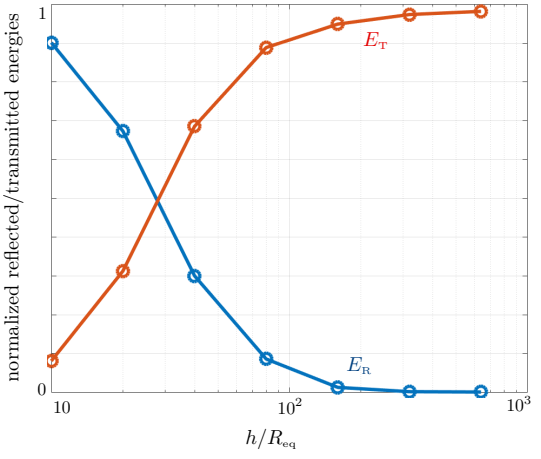

FIGURE 7. Normalized reflected and transmitted energies against h/R_{eq} ($\Delta P/P_{\mathrm{eq}} = 10^{-3}$).

values of $\Delta P/P_{\mathrm{eq}}$. The oscillations of the bubbles is clearly over-damped for this spacing. Next, the following trends are visible from these series: for larger ΔP (i) the direct part of reflected signal is smaller in amplitude, while the transmitted signal ressemble more and more to the initial pulse, (ii) the spectral content of the reflected signal is extended to higher frequencies and (iii) the damping of the oscillations is higher, which is visible by means of the signal propagating after the initial pulse has leaved the screen. In the non-linear regime of oscillation, pressure pulses with increasing amplitude produce more important bubble compression which possibly results in a weaken influence of the screen on the incident pulse. As a results the screen becomes invisible for large pressure amplitude, as illustrated in figure 9.

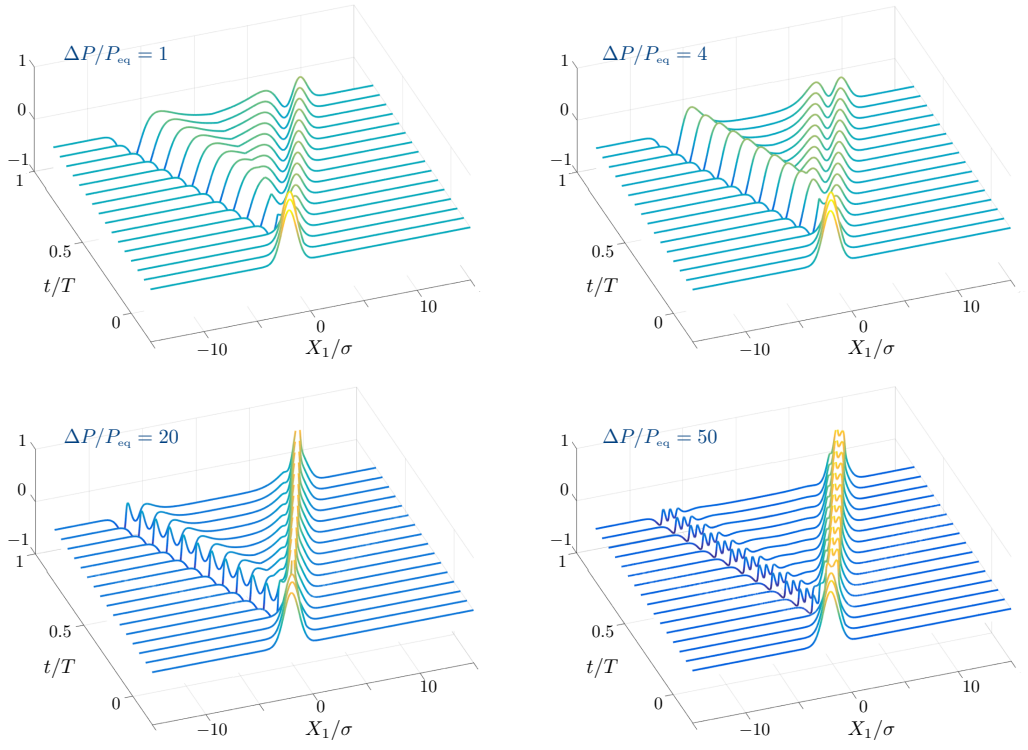

FIGURE 8. Propagation of an initial Gaussian pulse in the non-linear regime of oscillation for increasing $\Delta P/P_{eq}$.

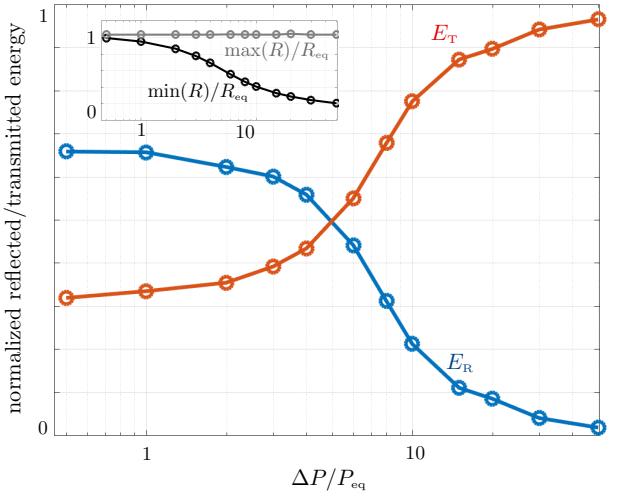

FIGURE 9. Normalized reflected and transmitted energies against $\Delta P/P_{eq}$ ($h/R_{eq} = 20$). The inset shows the minimum and maximum radii of $R(t)$ due to the compression of the bubbles by the incident pulse.

7. Concluding remarks

In this work, we have studied the interaction of acoustic waves with a screen made of a single layer of bubbles. We have obtained an effective screen model able to capture the effect of the bubbles by means of transmission conditions on the acoustic pressure and normal velocity. Although the derivation differs from that presented in Ng & Ting (1986) and Miksis & Ting (1989), the resulting model contains the same ingredients, namely a jump in the normal velocity coupled to an equation of the Rayleigh-Plesset type. The resulting coupling is accompanied by an exchange energy and it has been shown that the energy stored and then released by the bubbles is positive, hence the model is well suited for numerical implementation in the time domain. Next, the ability of the screen to interact with the fluid is measured by a non-dimensional parameter which involves a balance between the frequency regime $\omega R_{\rm eq}/c_\ell$, the relative bubble distance $R_{\rm eq}/h$ and the Mach number. The two first parameters measure the radiative damping of the bubbles which can be interpreted as an effective viscosity in the linear regime; the latter parameter is linked to the acoustic signal and it has been shown that strong linear oscillations can be observed even at very low Mach numbers.

The model is restricted to the low frequency regime and large contrast in the mass densities between liquid and gaz, which is physical since the Minnaert resonance occurs in this range of parameters. It is also restricted to low Mach numbers to prevent from non-linear propagation in the fluid and to relatively large distances between the bubbles. While the hypothesis of low Mach numbers could be removed, that of large spacings is less easy to relax within the present asymptotic approach; the same restriction appeared in Caflisch *et al.* (1985*a*) and Caflisch *et al.* (1985*b*) for bubbly liquid and in the extension to thin bubbly layers in Ng & Ting (1986) and Miksis & Ting (1989). It is linked to the physical fact that decreasing the spacing produces over-damped oscillations whose dynamics are dictated by their temporal exponential decay and not by the resonance frequency. It is likely that two different time scalings have to be introduced to reach this regime; besides, comparison with direct numerics and experiments should tell us if such improvement is necessary or to the contrary if the present approach is sufficient in practice.

Eventually, several extensions can be sought which implies different levels of difficulties. Accounting for the surface tension and for the viscosity of the liquid is straightforward and in view of the results in Miksis & Ting (1989), it makes little doubts that this will affect the Rayleigh-Plesset equation only. Accounting for a viscoelastic matrix rather than for a fluid is less straightforward depending on the considered viscoelastic model; however, it is of interest in view of the application to anechoic tiles based on bubble resonances.

Appendix A. Scattering coefficients in the linear regime

A second remark concerns the case where the oscillations are small, with $R(\mathbf{X}',t) = R_{\rm eq}+r(\mathbf{X}',t)$, and $|r| \ll R_{\rm eq}$. Then, from (5.2), the transmission condition for the velocity simplifies to

$$[\![U_1]\!] = \frac{4\pi R_{\rm eq}^2}{h^2}\,\dot r, \quad \text{with} \quad \rho_\ell R_{\rm eq}\left(\ddot r + \omega_{\rm M}^2\, r\right) = P_{\rm eq} - P_{|X_1=0}, \tag{A 1}$$

where the second relation makes the Minnaert resonance frequency $\omega_{\rm M} = \sqrt{3\rho_{\rm g}c_{\rm g}^2/(\rho_\ell R_{\rm eq}^2)}$ to appear. Eventually, if the source imposes a harmonic regime with $e^{-i\omega t}$ time depen-

dence, the condition further simplifies to

$$\left[\!\left[\frac{\partial P}{\partial X_1}\right]\!\right] = \frac{4\pi R_{\rm eq}}{h^2}\,\frac{\omega^2}{\omega_{\rm M}^2-\omega^2}(P_{\rm eq}-P_{|X_1=0}). \tag{A 2}$$

This leads to the scattering coefficients (R_θ, T_θ) for an incident plane wave at oblique incidence θ on the bubbly screen of the form

$$R_\theta = \frac{iKR_{\rm eq}}{\cos\theta\,((\omega_{\rm M}/\omega)^2-1)-iKR_{\rm eq}}, \quad T_\theta = 1+R_\theta, \tag{A 3}$$

with $K = 2\pi/(kh^2)$, in agreement with the findings of Bretagne *et al.* (2011) and Leroy *et al.* (2015). Note that in these references, two additional ingredients are taken into account heuristically, (i) the attenuation due to the viscosity through a damping coefficient and (ii) collective effects of the bubbles within the array through a geometrical (or cutoff) parameter. While the viscosity can be taken into account at the dominant order in the asymptotic analysis, accounting for the more subtil interactions between bubbles requires to conduct the analysis at higher orders.

REFERENCES

Ammari, H., Fitzpatrick, B., Gontier, D., Lee, H. & Zhang, H. 2017 A mathematical and numerical framework for bubble meta-screens. *SIAM Journal on Applied Mathematics* **77** (5), 1827–1850.

Bergamasco, L & Fuster, Daniel 2017 Oscillation regimes of gas/vapor bubbles. *International Journal of Heat and Mass Transfer* **112**, 72–80.

Bretagne, A., Tourin, A. & Leroy, V. 2011 Enhanced and reduced transmission of acoustic waves with bubble meta-screens. *Applied Physics Letters* **99** (22), 221906.

Caflisch, R.E., Miksis, M. J., Papanicolaou, G. C. & Ting, L. 1985*a* Effective equations for wave propagation in bubbly liquids. *Journal of Fluid Mechanics* **153**, 259–273.

Caflisch, R. E., Miksis, M. J., Papanicolaou, G. C. & Ting, L. 1985*b* Wave propagation in bubbly liquids at finite volume fraction. *Journal of Fluid Mechanics* **160**, 1–14.

Doc, Jean-Baptiste, Conoir, Jean-Marc, Marchiano, Régis & Fuster, Daniel 2016 Nonlinear acoustic propagation in bubbly liquids: Multiple scattering, softening and hardening phenomena. *The Journal of the Acoustical Society of America* **139** (4), 1703–1712.

Domenico, SN 1982 Acoustic wave propagation in air-bubble curtains in waterpart i: History and theory. *Geophysics* **47** (3), 345–353.

Gaunaurd, G. 1977 One-dimensional model for acoustic absorption in a viscoelastic medium containing short cylindrical cavities. *The Journal of the Acoustical Society of America* **62** (2), 298–307.

Leighton, T. G. 2004 Nonlinear bubble dynamics and the effects on propagation through near-surface bubble layers. In *AIP Conference Proceedings*, , vol. 728, pp. 180–193. AIP.

Leroy, V., Strybulevych, A., Lanoy, M., Lemoult, F., Tourin, A. & Page, J.H. 2015 Superabsorption of acoustic waves with bubble metascreens. *Physical Review B* **91** (2), 020301.

Leroy, V., Strybulevych, A., Scanlon, M.G. & Page, J.H. 2009 Transmission of ultrasound through a single layer of bubbles. *The European Physical Journal E: Soft Matter and Biological Physics* **29** (1), 123–130.

Lombard, Bruno, Maurel, Agnes & Marigo, Jean-Jacques 2017 Numerical modeling of the acoustic wave propagation across a homogenized rigid microstructure in the time domain. *Journal of Computational Physics* **335**, 558–577.

Marigo, Jean-Jacques & Maurel, Agnès 2016 Homogenization models for thin rigid structured surfaces and films. *The Journal of the Acoustical Society of America* **140** (1), 260–273.

Miksis, Michael J & Ting, Lu 1989 Effects of bubbly layers on wave propagation. *The Journal of the Acoustical Society of America* **86** (6), 2349–2358.

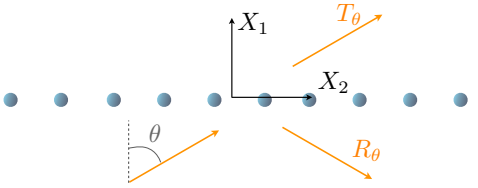

FIGURE 10. Scattering of an incident plane wave in the time-harmonic regime. In the effective problem, the bubbly screen is replaced by the transmission conditions (A 2) (with P continuous).

NG, KC & TING, L 1986 Wave propagation through a thin bubbly layer. *The Journal of the Acoustical Society of America* **79** (4), 924–926.

SHARMA, G. S., SKVORTSOV, A., MACGILLIVRAY, I. & KESSISSOGLOU, N. 2017 Acoustic performance of gratings of cylindrical voids in a soft elastic medium with a steel backing. *The Journal of the Acoustical Society of America* **141** (6), 4694–4704.

VAN WIJNGAARDEN, L. 1968 On the equations of motion for mixtures of liquid and gas bubbles. *Journal of Fluid Mechanics* **33** (3), 465–474.

Appendix A. The linear harmonic solution

A second remark concerns the case where the oscillations are small, with $R(\mathbf{X}', t) = R_{\rm eq} + r(\mathbf{X}', t)$, and $|r| \ll R_{\rm eq}$. Then, from (5.2), the transmission condition for the velocity simplifies to

$$[\![U_1]\!] = \frac{4\pi R_{\rm eq}^2}{h^2}\,\dot r, \quad \text{with} \quad \rho_\ell R_{\rm eq}\left(\ddot r + \omega_{\rm M}^2\, r\right) = -P(0,t), \tag{A 1}$$

where the second relation makes the Minnaert resonance frequency $\omega_{\rm M} = \sqrt{3\rho_{\rm g} c_{\rm g}^2/(\rho_\ell R_{\rm eq}^2)}$ to appear. Eventually, if the source imposes a harmonic regime with $e^{-i\omega t}$ time dependence, the condition further simplifies to

$$\left[\!\!\left[\frac{\partial P}{\partial X_1}\right]\!\!\right] = -\frac{4\pi R_{\rm eq}}{h^2}\,\frac{\omega^2}{\omega_{\rm M}^2 - \omega^2}\,P(0,t). \tag{A 2}$$

This leads to the scattering coefficients (R_θ, T_θ) for an incident plane wave at oblique incidence θ on the bubbly screen of the form

$$R_\theta = \frac{iKR_{\rm eq}}{\cos\theta\,((\omega_{\rm M}/\omega)^2 - 1) - iKR_{\rm eq}}, \quad T_\theta = 1 + R_\theta, \tag{A 3}$$

with $K = 2\pi/(kh^2)$, in agreement with the findings of Bretagne *et al.* (2011) and Leroy *et al.* (2015). Note that in these references, two additional ingredients are taken into account heuristically, (i) the attenuation due to the viscosity through a damping coefficient and (ii) collective effects of the bubbles within the array through a geometrical (or cutoff) parameter. While the viscosity can be taken into account at the dominant order in the asymptotic analysis, accounting for the more subtil interactions between bubbles requires to conduct the analysis at higher orders. Also more demanding is to develop an analysis valid at or very close to the resonance, namely for vanishing $\eta = \omega - \omega_{\rm M}$. As in Caflisch *et al.* (1985*b*), our present asymptotic analysis holds for a fixed η and $\varepsilon \to 0$.